Scanning Electrochemical Cell Microscopy: Theory and Experiment for Quantitative High Resolution Spatially-Resolved Voltammetry and Simultaneous Ion-Conductance Measurements

ARTICLE *in* ANALYTICAL CHEMISTRY · MARCH 2012

Impact Factor: 5.64 · DOI: 10.1021/ac203195h · Source: PubMed

8 AUTHORS, INCLUDING:

Stanley C.S. Lai
University of Twente
31 PUBLICATIONS **1,021** CITATIONS
SEE PROFILE

Kim Mckelvey
University of Utah
42 PUBLICATIONS **528** CITATIONS
SEE PROFILE

Neil Ebejer
The University of Warwick
13 PUBLICATIONS **386** CITATIONS
SEE PROFILE

Alex W. Colburn
The University of Warwick
44 PUBLICATIONS **528** CITATIONS
SEE PROFILE

analytical chemistry

Article

pubs.acs.org/ac

Scanning Electrochemical Cell Microscopy: Theory and Experiment for Quantitative High Resolution Spatially-Resolved Voltammetry and Simultaneous Ion-Conductance Measurements

Michael E. Snowden,[†] Aleix G. Güell,[†] Stanley C. S. Lai,[†] Kim McKelvey,[‡] Neil Ebejer,[†] Michael A. O'Connell,[†] Alexander W. Colburn,[†] and Patrick R. Unwin*[,†]

[†]Department of Chemistry, and [‡]MOAC Doctoral Training Centre, University of Warwick, Coventry CV4 7AL, United Kingdom

Supporting Information

ABSTRACT: Scanning electrochemical cell microscopy (SECCM) is a high resolution electrochemical scanning probe technique that employs a dual-barrel theta pipet probe containing electrolyte solution and quasi-reference counter electrodes (QRCE) in each barrel. A thin layer of electrolyte protruding from the tip of the pipet ensures that a gentle meniscus contact is made with a substrate surface, which defines the active surface area of an electrochemical cell. The substrate can be an electrical conductor, semiconductor, or insulator. The main focus here is on the general case where the substrate is a working electrode, and both ion-conductance measurements between the QRCEs in the two barrels and voltammetric/amperometric measurements at the substrate can be made simultaneously. In usual practice, a small perpendicular oscillation of the probe with respect to the substrate is employed, so that an alternating conductance current (ac) develops, due to the change in the dimensions of the electrolyte contact (and hence resistance), as well as the direct conductance current (dc). It is shown that the dc current can be predicted for a fixed probe by solving the Nernst−Planck equation and that the ac response can also be derived from this response. Both responses are shown to agree well with experiment. It is found that the pipet geometry plays an important role in controlling the dc conductance current and that this is easily measured by microscopy. A key feature of SECCM is that mass transport to the substrate surface is by diffusion and, for charged analytes, ion migration which can be controlled and varied quantifiably via the bias between the two QRCEs. For a working electrode substrate this means that charged redox-active analytes can be transported to the electrode/solution interface in a well-defined and controllable manner and that relatively fast heterogeneous electron transfer kinetics can be studied. The factors controlling the voltammetric response are determined by both simulation and experiment. Experiments demonstrate the realization of simultaneous quantitative voltammetric and ion conductance measurements and also identify a general rule of thumb that the surface contacted by electrolyte is of the order of the pipet probe dimensions.

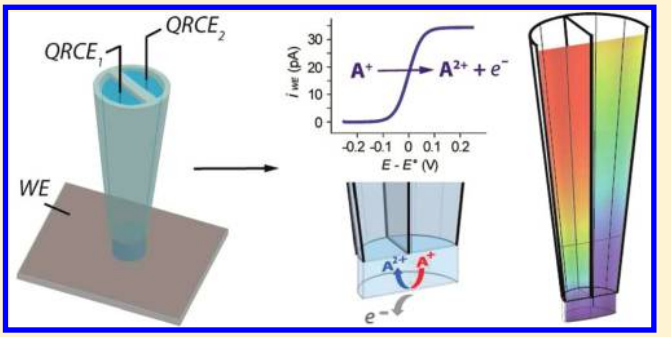

We have recently introduced scanning electrochemical cell microscopy (SECCM)[1,2] as a new scanning electrochemical probe microscopy technique,[3,4] to facilitate simultaneous high resolution topographical, conductometric, and amperometric/voltammetric imaging of surfaces and interfaces. SECCM is the latest development in a succession of innovations in scanning electrochemical probe microscopy, starting with scanning electrochemical microscopy (SECM),[5−5] and expanded to techniques such as SECM-atomic force microscopy (AFM),[6] shear force-SECM,[7] alternating current (ac)-SECM,[8] intermittent contact (IC)-SECM,[9] SECM-scanning ion conductance microscopy (SICM),[10] and various scanning droplet techniques,[11] including the scanning micropipet contact method (SMCM),[12] and related methods.[13]

The probe in SECCM is a theta pipet, pulled to a sharp point. Each of the two compartments (Figure 1 (a)) is filled with an electrolyte solution, which forms a meniscus at the pipet tip, and each contains a quasi-reference counter electrode (QRCE), often a chloridized silver wire.[1] A potential difference applied between the QRCEs results in the migration of ions between the two barrels, through the meniscus that protrudes from the end of the pipet. The electrochemical probe is mounted on a high resolution (piezo-electric) positioning system, and a sinusoidal oscillation is applied to the *z*-position of the piezo-electric positioner in the direction of the axis of the pipet (normal to the surface of interest), with an oscillation amplitude of a small fraction of the pipet diameter. Contact of the meniscus at the end of the pipet with the surface can be detected by the sudden development of an alternating conductance current (ac) between the barrels, due to the dynamic motion of the thin layer of electrolyte trapped

Received: December 10, 2011
Accepted: January 26, 2012

   dx.doi.org/10.1021/ac203195h | *Anal. Chem.* XXXX, XXX, XXX−XXX

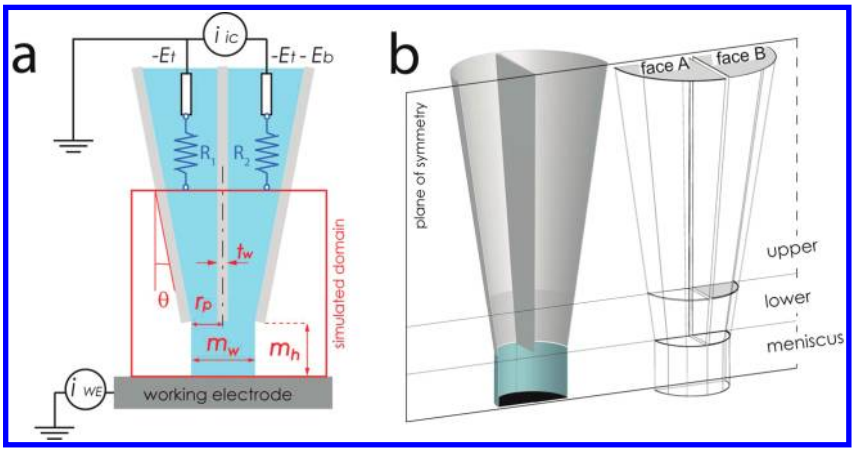

Figure 1. Schematics of (a) the SECCM setup showing the key geometric dimensions and electronic circuits and (b) the simulation domain. Not to scale.

between the end of the pipet and the surface.[1,2,14] Once landed the tip can be scanned across the surface, keeping the tip to sample distance fairly constant, by using the ac conductance signal as a feedback parameter. A new enhancement we describe herein is the ability to "tune" and vary the tip to sample distance and carry out approach curve measurements in which various current responses are measured as the electrolyte layer is compressed.

The direct current (dc) conductance signal between the two QRCEs in SECCM is sensitive to ion uptake and release from surfaces, as evidenced by studies of calcium phosphate uptake by enamel surfaces.[1] For investigations of conducting or semiconducting substrates, a key aspect of SECCM is the ability to also directly carry out local surface electrochemistry measurements (e.g., voltammetry, amperometry, *etc.*). In this situation, the pipet and substrate constitute a microscopic (or nanoscopic) electrochemical cell, with the substrate as a working electrode and one of the QRCEs acting as the counter/reference electrode for voltammetic/amperometric measurements (*vide infra*). The ion-conductance measurements mentioned above can still be made simultaneously. Indeed, a particularly interesting aspect of SECCM is the possibility of making surface voltammetic/amperometric measurements, and simultaneous conductometric measurements, thereby greatly enhancing the information content of local dynamic electrochemical experiments. This aspect is considered herein. The capabilities of SECCM, in this context, are well illustrated by initial studies[1] and our recent investigations of the electrocatalytic activity of individual Pt nanoparticles.[2]

As with SMCM,[12] the pipet probe of SECCM provides high intrinsic diffusion rates to local features on a substrate surface, because there is some nonlinear diffusion inherent in the tapered pipet probe design, which is defined by the semiangle, θ (Figure 1 (a)). When the substrate is a conductor or (semiconductor), as considered herein, the pipet probe thus delivers high rates of mass transport to a small working electrode area, such that the format is essentially that of an 'ultramicroelectrode' (UME). This means that a wide range of substrates can be studied on a local scale, and with high rates of diffusion, without having to physically construct or manufacture an UME. As highlighted herein, for charged analytes, SECCM offers the further possibility of controlling and varying mass transport via the applied potential between the two QRCEs.

The aim of this paper is to provide a comprehensive model for mass transport in SECCM, including the ion conductance characteristics and the voltammetric response with a conducting electrode substrate. The study of conducting/semiconducting materials is expected to be a major application area for SECCM, but the results presented are also valuable for determining the main features of mass transport in SECCM and how these may be controlled and characterized for other types of substrates. Moreover, with the recent increase in the use of various micropipet and nanopipet imaging methods,[11,12,14,15] we expect the results to be of general utility. Finite element method (FEM) modeling is utilized to determine the electric field within the SECCM pipet and meniscus and to accurately describe mass transport. The predictions of the simulations are examined by experiments, thus providing a strong, quantitative foundation for the future application of SECCM for spatially resolved measurements.

EXPERIMENTAL SECTION

SECCM measurements were performed using the system originally reported by Ebejer et al.,[1] but modified slightly, so that the conductometric and amperometric measurements could each be made with independent potential control (Figure 1(a)). High sensitivity home-built current to voltage converters (amplifiers) were used to measure the current between the QRCEs in the barrels of the theta pipet (i_b) and the substrate working electrode current (i_{we}). The entire experimental assembly was installed in a Faraday cage. Instrument control and data acquisition utilized a PC with a FPGA card (PCI-7830R, National Instruments) with a LabVIEW 9.0 interface (National Instruments). Cyclic voltammetry (CV) experiments were carried out by sweeping the potential at the QRCEs ($-E_t$) while maintaining the bias between the barrels (E_b) as shown in Figure 1 (a). The most driving QRCE acts as the counter electrode for the redox process at the substrate (working) electrode. Note that in this report i_{we} is 2 orders of magnitude lower than the barrel ion conductance current, i_b, although it may be important to take account of this when analyzing experimental ion conductance barrel currents for diagnostic purposes (*vide infra*).

Dual barrel borosilicate glass theta capillaries (o.d. 1.5 mm, i.d. 0.23 mm, Harvard Apparatus, UK) were pulled using a laser puller (Model P-2000, Sutter Instruments, USA) to produce tapered pipets of approximately 1 μm total diameter at the end

dx.doi.org/10.1021/ac203195h | *Anal. Chem.* XXXX, XXX, XXX–XXX

(*vide infra*). Typically, pipets had dimensions of r_p = 400 nm−600 nm and θ = 6.5°−8.5° (Figure 1 (a)) and were measured accurately (by field emission-scanning electron microscopy (FE-SEM), Supra 55-VP Zeiss).[16] The outer walls of the pipets were silanized[17] with dimethyldichlorosilane to ensure a reasonable confinement of the protruding meniscus to the very end of the pipet (confirmed in Supporting Information section S1).

Both barrels of the pipet were filled with the solution of interest. For the experimental studies reported, this was a 2 mM solution of the redox mediator, the hexafluorophosphate salt of trimethyl(ferrocenylmethyl) ammonium, $FcTMA^+$ (synthesized in house),[18] in an aqueous solution of KCl, with a concentration range from 2 mM to 0.1 M (Fischer, analytical grade). All solutions were prepared using Milli-Q water (Millipore Corp.) with a resistivity of 18.2 MΩ cm at 25 °C. Chloridized silver wires (Ag/AgCl) were inserted into each barrel and acted as the QRCEs. Highly oriented pyrolytic graphite (HOPG) (SPI supplies, West Chester, PA − SPI1), freshly cleaved immediately prior to measurements, provided a clean and flat working electrode substrate for surface electrochemistry measurements. To minimize evaporation from the end of the pipet, the sample was mounted in a humidified cell with a saturated KCl solution moat.[1]

The electrochemical (voltammetric) experiments were performed at a series of positions on the HOPG substrate, utilizing the *z*-piezo to approach the probe toward the sample until a contact of the meniscus and surface was attained. Control experiments demonstrated that closely similar voltammograms were obtained with the pipet oscillating in contact with the surface (oscillation amplitude 100 nm, frequency 300 Hz) and without oscillation. Voltammetric measurements were typically made with a static probe for comparison to the developed model, but note that the model for the dc ion-conductance current and voltammetry developed herein is applicable to oscillating probes for the range of amplitudes and frequencies defined hitherto[1,2] and herein.

THEORY AND SIMULATIONS

All simulations were performed using the FEM modeling package Comsol Multiphysics 4.1 (Comsol AB, Sweden) with MatLab 2009b (Mathworks Inc., Cambridge) interface. Figure 1 (b) illustrates the simulation domain which represents half of a pulled theta pipet and the meniscus, making use of the symmetry plane perpendicular to the wall that divides the pipet into two barrels, in order to enhance computational efficiency. To optimize the calculations, each barrel was divided into 2 sections, labeled 'upper' and 'lower' in Figure 1 (b). These sections were used to manage the mesh, such that the mesh in the meniscus and lower sections of the barrels, where the concentration and potential gradients experienced were steepest (*vide infra*), were much finer than in the upper section. Overall, the pipet was conical with a circular base, and the dividing segment separating the barrels was located at the center. The diameter of the meniscus contacting the working electrode (m_w) was usually approximated to be the same as the pipet diameter, except for studies concerning the effect of the meniscus shape on the current at the working electrode, i_{we}, and the ion-conductance current between the barrels, i_{ic}. As shown through the studies herein, electrolyte contact of the surface of the order of the pipet (inner) diameter is a good rule of thumb. The geometrically significant parameters, as highlighted in Figure 1 (a) and (b), are the inner radius of the capillary, r_p, the central segment thickness, t_w, and the semiangle of the capillary, θ (°). Additionally, the meniscus height, m_h, can be important, and we outline how this parameter can be deduced from the various SECCM current responses. We simulate a static probe but show how data derived can be used to treat an oscillating probe.

PIPET ELECTRIC FIELD AND MIGRATION IN SECCM

We first consider the current flow between the two QRCEs in SECCM, initially ignoring any processes at the substrate electrode. The time-dependent Nernst−Planck equation (eq 1) with electroneutrality (eq 2) was solved for all species within the pipet

$$\frac{\partial c_j}{\partial t} + \nabla(-D_j\nabla c_j - z_j u_j F c_j \nabla V) + \mathbf{u}\nabla c_j = 0 \quad (1)$$

$$\sum_j z_j c_j = 0 \quad (2)$$

where c_j, D_j, z_j, and u_j are the concentration, diffusion coefficient, charge, and ionic mobility of species, *j*, respectively, *t* is time, *F* is the Faraday constant, *V* is the electric field (provided by the bias, E_b, between the QRCEs in the two barrels), and **u** is the velocity vector of the solution within the pipet. To simplify the problem we have ignored convective terms (**u** = 0) that might contribute, for example by electroosmotic flow, which is reasonable given the high rates of migration in SECCM (and diffusion for the case where the substrate working electrode is active) compared to the electroosmotic flow rate predicted by the Smoluchowski equation (Supporting Information, section S2).[19] Consequently, other factors[20] are negligible for the system considered. Note that for this particular stage of the problem, a steady-state response is observed, but we solved the time-dependent electric field for compatibility with the time dependent substrate working electrode boundary condition discussed later.

The model simulates the movement of up to five ionic species within the pipet and meniscus: K^+, Cl^-, $FcTMA^+$, $FcTMA^{2+}$, and PF_6^- but could be extended to any practical number of species where the mobility, diffusion coefficient, and charge are known. Values for u_j were determined from the molar conductance (λ_j) for the relevant ions. For K^+, Cl^-, and PF_6^- reasonable values for the conditions used herein were as follows:[21] λ_{K^+} = 73.2 S cm^2 mol^{-1}, λ_{Cl^-} = 70.3 S cm^2 mol^{-1}, $\lambda_{PF_6^-}$ = 56.9 S cm^2 mol^{-1}. The values for $FcTMA^+$ and $FcTMA^{2+}$ were derived from D_j = 6.0 × 10^{-6} cm^2 s^{-1} giving λ_j = 22.5 S cm^2 mol^{-1} in each case (see Supporting Information section S2 for further details).[22]

The simulation assumes that the applied electric field is uniform across faces A and B (Figure 1 (b)), which is reasonable due to the large area of the faces compared to the cross-sectional area of the end of the pipet and the distance from the substrate surface to the end of the pipet. For the purpose of the simulation, it was convenient to set the potential, *E*, at face A of the capillary to 0 V (eq 3), while face B was set to a theoretical bias potential of E_f (eq 4). Note that this potential difference is less than that applied experimentally, E_b, due to the finite resistances, R_1 and R_2 (Figure 1 (a)), in the remainder of the pipet shaft. Faces A and B are each governed by an inflow boundary condition as described by eq 5 representing the movement of ions into and out of the simulated domain. Under typical experimental conditions

dx.doi.org/10.1021/ac203195h | *Anal. Chem.* XXXX, XXX, XXX−XXX

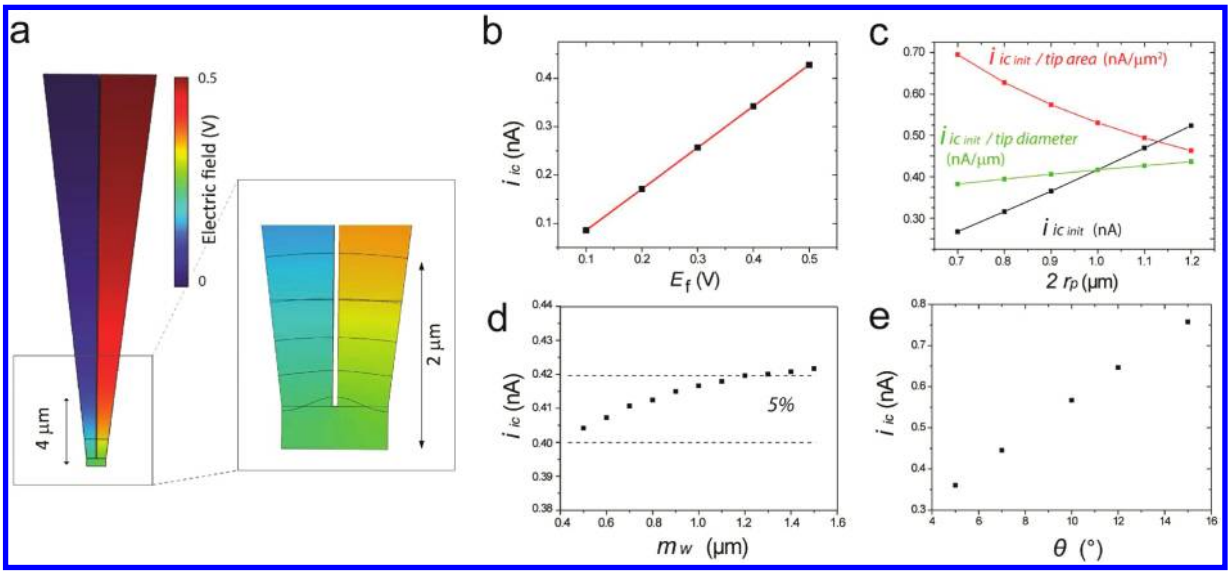

Figure 2. (a) Simulation of the electric field within a pipet of r_p = 0.5 μm, θ = 7°, and m_h = 0.4 μm, with E_f = 0.5 V. Plots demonstrating the dependence of migration current on bias potential (b), pipet radius (c), meniscus contact radius (d), and semiangle (e). In all cases the solution contained 1 mM KCl, and values for all parameters (unless a variable) are as defined for (a) and in the text.

evaporation from the meniscus is prevented by a humidity cell, hence the meniscus walls are simulated as no flux boundaries (eqs 6 and 7). The remaining faces of the pipet are also subject to boundary conditions which stipulate no normal flux of species across the boundary and no normal change in the electric field, described with eq 6 and eq 7, respectively

$$\text{Face A:} \quad E = 0 \tag{3}$$

$$\text{Face B:} \quad E = E_f \tag{4}$$

$$\text{Bulk solution:} \quad c_j = c_{j,init} \tag{5}$$

$$\text{No normal flux/Symmetry:} \quad \mathbf{n}.\mathbf{N}_j = 0 \tag{6}$$

$$\text{No normal flux/Symmetry:} \quad \mathbf{n}.\mathbf{N}^V = 0 \tag{7}$$

where $\mathbf{n}$ is the unit normal vector, $\mathbf{N}_j$ is the flux vector of species j, and $\mathbf{N}^V$ is the potential field vector. The subscript '*init*' signifies an initial condition (*i.e.* t = 0).

EXTENSION TO SECCM VOLTAMMETRY

The simulation was extended to include an electrochemical reaction on the substrate working electrode. We considered the one-electron oxidation of $FcTMA^+$ to $FcTMA^{2+}$ (eq 8) as both a reversible (Nernstian) process and with Butler–Volmer kinetics

$$FcTMA^+ \underset{k_f}{\overset{k_b}{\rightleftharpoons}} FcTMA^{2+} + e^- \tag{8}$$

For the model developed, the double layer was sufficiently small (~1 nm) compared to the liquid meniscus height (m_h in Figure 1 (a)) that the working electrode potential does not perturb the electric field within the meniscus. This is a reasonable assumption[23,24] for the conditions used herein. Further details on the boundary conditions for these simulations are given in the Supporting Information (S2).

RESULTS AND DISCUSSION

Migration within the SECCM Probe. It is instructive to first consider the steady electric field and migration of species within the theta pipet with no reaction occurring at the working electrode. Figure 2 (a) shows the potential field for a bias of 0.5 V between faces A and B, for a pipet of r_p = 0.5 μm, θ = 7°, and m_h = 0.4 μm. For simplicity and illustrative purposes we assume the solution between the tip and surface to have a cylindrical geometry, which is reasonable based on the data in Supporting Information (Figure S1) and previous work.[1,2,25] The largest change in the potential field is observed within a few micrometers of the pipet tip, and it is evident that the approximation of uniform potential fields applied across faces A and B (Figure 1 (b)) is reasonable because, for most of the pipet, the field is uniform across the width of a barrel. The potential gradient experienced at the end of the tip is due to the resistance at the pipet tip being significantly larger than the resistance further up the barrels, due to the decrease of the cross-sectional area at the end of the pipet. Note that the substrate experiences a uniform potential of E_t+(E_b/2), the midpoint of the potential applied to the QRCEs.

Simulations to determine the dependence of the migration current on the bias potential, tip radius, meniscus contact radius, and the semiangle were carried out for tips containing 1 mM KCl, as an illustrative case. Figure 2 (b)-(e) summarizes data for a typical SECCM pipet geometry with E_f = 0.5 V, r_p = 0.5 μm, m_h = 0.4 μm, θ = 7° unless one of these parameters is the variable. Figure 2 (b) shows that there is a linear (ohmic) relationship between the bias potential and the migration current. Simulations for pipets with a range of radii from 0.35–0.6 μm (Figure 2 (c)) show that, as the tip radius decreases, the migration current decreases, due to a reduction in the cross-sectional area of the pipet and the concurrent increase in the overall resistance. Interestingly, the migration current has a close to linear dependence on the radius of the pipet (Figure 2 (c)) as seen for diffusion/migration to a micro disk.[26]

To investigate meniscus contact effects, the meniscus geometry was approximated to have a linear liquid/air interface (for simplicity and computational ease), and simulations were

dx.doi.org/10.1021/ac203195h | *Anal. Chem.* XXXX, XXX, XXX–XXX

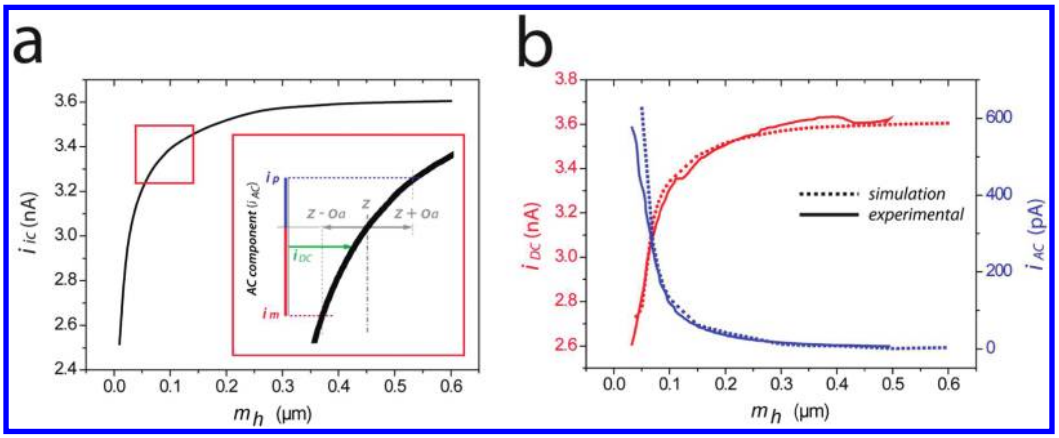

Figure 3. (a) Simulated approach curve of i_{ic} vs m_h for a nonoscillating SECCM pipet with r_p = 0.5 μm, θ = 7°, E_f = 0.092 V filled with 50 mM KCl. Inset defines parameters to predict the response for an oscillating pipet; see text for a detailed description. (b) Comparison of experimental i_{AC} and i_{DC} approach curves and corresponding simulations for a pipet with r_p = 0.5 μm, θ = 7° filled with 50 mM KCl oscillating in the z direction at 100 Hz and 100 nm peak to peak amplitude.

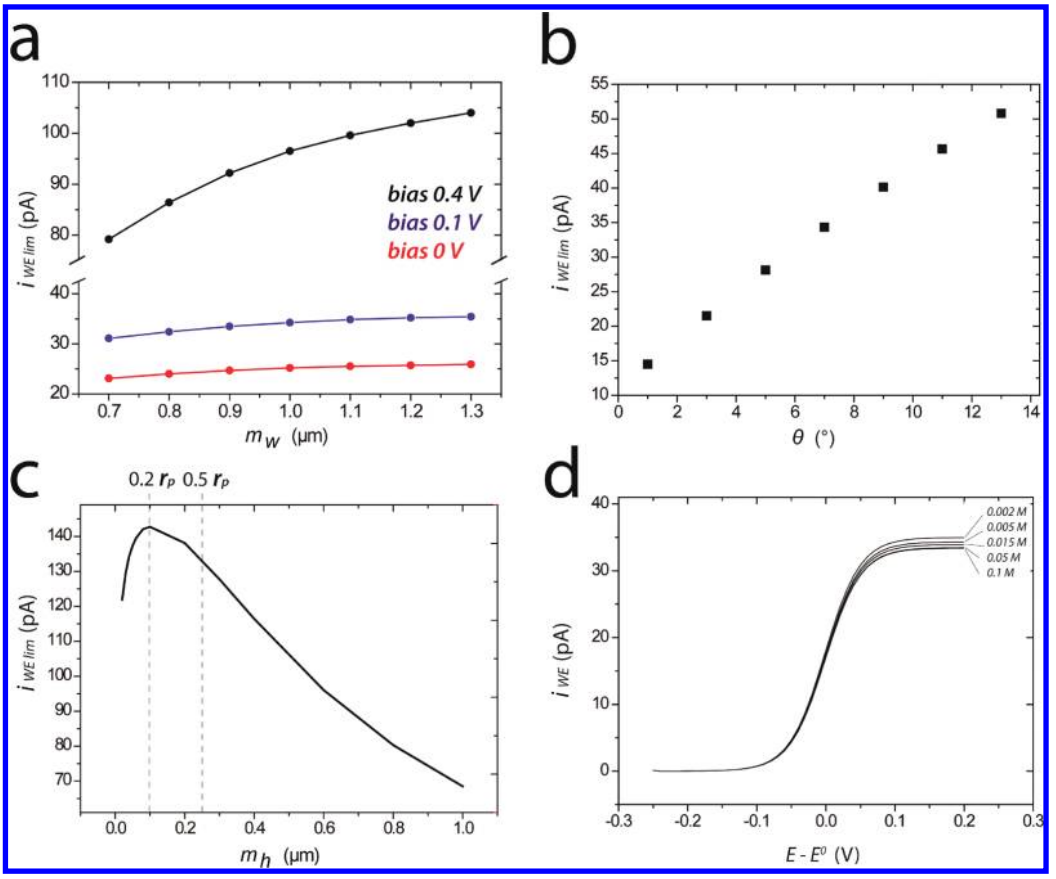

Figure 4. FEM data showing the dependence of the working electrode limiting current on the meniscus contact diameter (a) and the semiangle (b) for a SECCM probe with r_p = 0.5 μm, m_h = 0.4 μm, containing 2 mM $FcTMA^+$ and 5 mM KCl. The bias, E_f, considered is marked on (a) and for (b) E_f = 0.1 V. (c) The dependence of the working electrode limiting current response on the tip/substrate separation, m_h. (d) The effect of the supporting electrolyte concentration (as marked) on the voltammetric response, with all parameters as in part (c) and m_h = 0.4 μm.

performed with a (typical) tip−substrate separation of 0.4 and 1 μm overall tip inner diameter ($2r_p$). In Figure 2 (d) the migration current is plotted as a function of the meniscus contact radius, showing a change in the migration current of less than 5% for a contact diameter of 0.5−1.5 μm with a diameter of 1−1.5 μm showing barely any change. This behavior is because the region of the liquid in the contacting droplet close to the tip end has the greatest influence on the resistance (Figure 2 (a)). These results thus confirm that approximating the meniscus to a cylinder for electric field calculations and ion conductance measurements is reasonable for the typical tip heights encounterd in SECCM.

Figure 2 (e) shows a dramatic increase of resistance (decrease in migration current) as the semiangle decreases, emphasizing that this parameter needs to be measured accurately for the quantitative deployment of SECCM. In

dx.doi.org/10.1021/ac203195h | Anal. Chem. XXXX, XXX, XXX−XXX

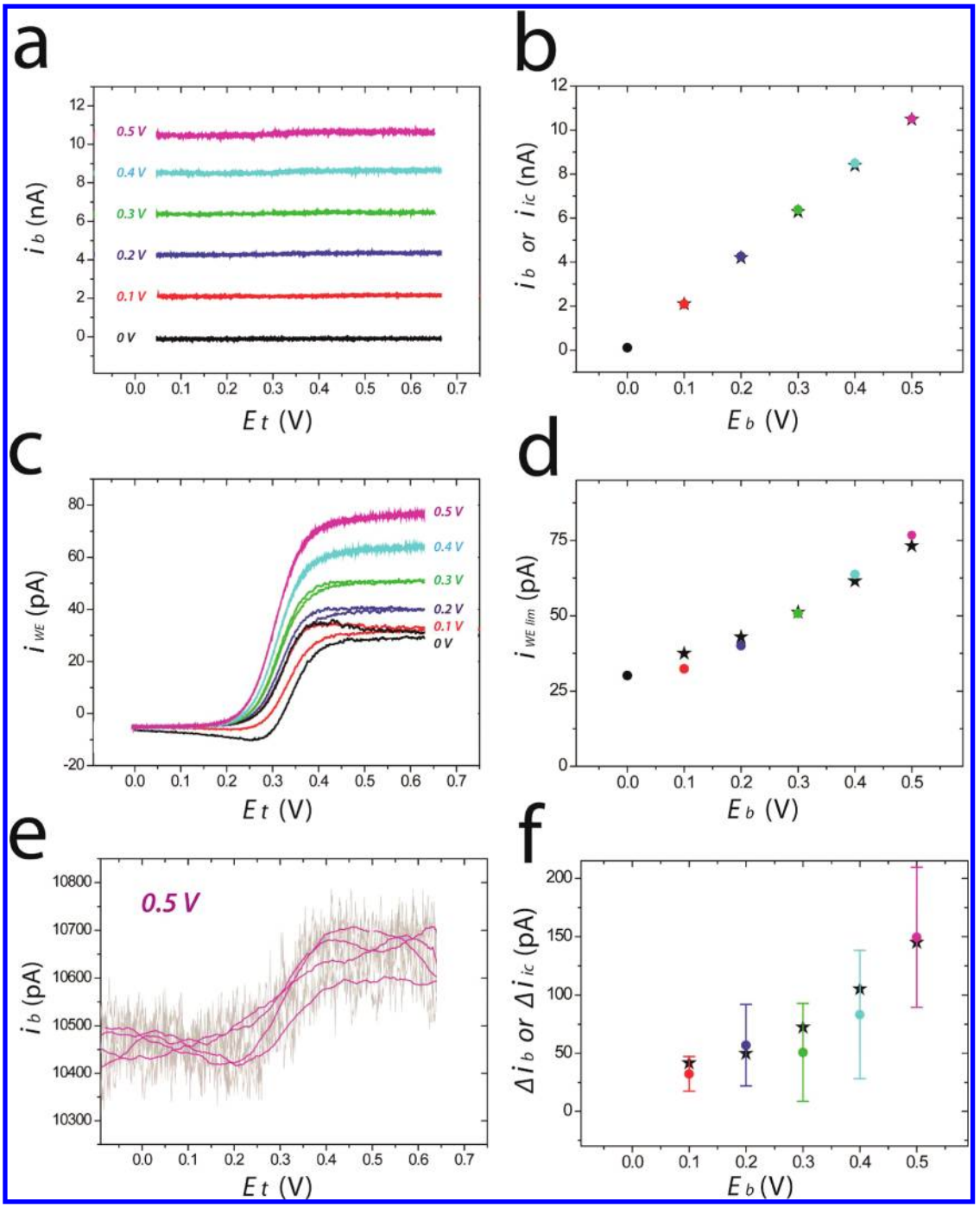

Figure 5. Simultaneously recorded ion conductance currents (a,b) and the working electrode response (c,d) during CV measurements (ν = 100 mV s^{-1}) for the $FcTMA^{+/2+}$ couple at HOPG. The currents between barrels (experimentally i_b and simulated i_{ic} (a,b)) and the working electrode response (i_{WE} and $i_{WE,\,lim}$) were recorded as a function of E_t for different values of E_b between 0 and 0.5 V (marked on (a) and (c)). The probe was defined by r_p = 0.6 μm and θ = 8.5°, m_h = 0.15 μm filled with 2 mM $FcTMA^+$ and 50 mM KCl. Plot (e) is a magnified view of the current between barrels, i_b, at bias 0.5 V (from plot (a)), where a change in i_b is observed. The change in i_{ic} during voltammetric sweeps is plotted as a function of the bias potential for experimental and simulated data sets (f). Experimental data (colored circles) and simulated data (stars) are plotted for (b), (d), and (f).

summary, Figure 2 (c)−(e) shows that the migration current at a typical tip/substrate separation of 0.4 μm is dominated by the pipet tip radius and the semiangle, which are physical parameters that are easily by measured by FE-SEM.

SECCM Approach Curves. Figure 3 (a) shows the simulated effect of the tip−substrate separation on the barrel ion-conductance current for a pipet of r_p = 0.5 μm, θ = 7°, E_f = 0.092 V filled with 50 mM KCl. These parameters were consistent with the pipet dimensions used for the experimental data in Figure 3 (b). E_f was determined by matching the simulated ion conductance current, i_{ic}, to the experimental barrel current, i_b, to take account of the potential drop from the QRCEs to faces A and B due to R_1 and R_2. The liquid contact was considered to be a cylinder with a radius the same size as the pipet. As the height of the pipet above the substrate decreases, the current between the barrels decreases due to the

dx.doi.org/10.1021/ac203195h | Anal. Chem. XXXX, XXX, XXX−XXX

increasing resistance within the meniscus, but - consistent with the data in Figure 2 (a) and for SICM[27] - this effect is only significant at very small pipet-substrate separations (below *ca.* $0.5r_p$).

Experimentally, the pipet is typically oscillated on approach to a substrate,[1,2,24] providing an alternating current signal (i_{AC}) and an average direct current signal (i_{DC}). These currents can be predicted from the simulated ion-conductance (i_{ic}) approach curve. As shown in Figure 3 (a) the ion-conductance current (i_{ic}) at height $z + o_a$ is i_p and at $z - o_a$ is i_m, so $i_{DC} = (i_p+i_m)/2$, and the peak-to-peak ac amplitude, $i_{AC} = i_p - i_m$. Clearly for a small oscillation amplitude, i_{DC} is close in magnitude to i_{ic}.

Figure 3 (b) shows typical experimental approach curves of i_{DC} and i_{AC} recorded as an SECCM pipet (r_p = 0.5 μm, θ = 7°, E_b = 0.5 V filled with 50 mM KCl and oscillated at a frequency of 100 Hz and an amplitude of 100 nm peak to peak) was lowered from air toward a borosilicate surface, with which it made contact, and the approach was continued to determine how the values of i_{AC} and i_{DC} changed as the meniscus height was compressed. The experimental data confirm the simulations. When the pipet is at a height of $0.5r_p$, or greater from the surface, i_{DC} tends to a maximum value. As the pipet is approached to less than 0.25 μm (*ca.* $0.5r_p$) above the substrate, the barrel current decreases significantly and the corresponding ac component increases for decreasing tip to substrate separations. The experimental and simulated data for both i_{DC} and i_{AC} as a function of pipet height in Figure 3 (b) illustrate that the separation between the pipet and the substrate surface can be accurately characterized by these types of approach curves, which can be stopped at a desired value of i_{DC} and/or i_{AC}.

Surface Electrochemistry in SECCM. We now turn to the case where the substrate is a working electrode and voltammetric measurements are made using SECCM. For illustrative purposes, a pipet with r_p = 0.5 μm, m_h = 0.4 μm, containing 2 mM $FcTMA^+$ and 5 mM KCl, with three E_f values of 0 V, 0.1 V, and 0.4 V, was simulated. We first focus on the limiting current response, $i_{WE,\,lim}$. The impact of the meniscus contact area, m_w, on the working electrode response for a pipet with θ = 7° is shown in Figure 4 (a). In general, the working electrode current increases as the substrate area increases. However, the change in current is greatest for meniscus contact diameters less than the pipet diameter and is seen most for high bias between the 2 QRCEs. This is because the bias potential between the QRCEs serves to drive the charged redox species (in this case) toward the working electrode surface so that the concentration gradient becomes compressed within the very end of the tip and meniscus, where the influence of the potential field is strongest (see Figure 2 (a) for example). For neutral redox-active species or when there is no applied bias (0 V in Figure 4 (a)) mass transport in SECCM is by diffusion only and thus similar to SMCM, discussed in detail previously.[12] It follows from the data in Figure 4 (a) that one can use the limiting current response for a redox reaction to provide additional insight on the pipet and meniscus geometry, particularly if one can record tip approach curve measurements.

The effect of changing the semiangle of the pipet has a much more dramatic effect on the limiting current, as shown in Figure 4 (b), mirroring the behavior for the conductance current (Figure 2 (e)). As the semiangle increases there is an increased radial contribution to mass transport, increasing the limiting current.

The effect of meniscus height, m_h, on the working electrode limiting current response is shown in Figure 4 (c). For heights greater than *ca.* $0.5r_p$, the working electrode limiting-current increases as the height decreases, because of the increasing effect of the electric field between the 2 barrels (*vide supra*). However, for $0 \le m_h \le 0.2r_p$, the current decreases as the height decreases, because in this region there is a dramatic decrease in migration current with height (see for example Figure 3 (a)), and this has a significant impact on the overall mass transport to the substrate surface. There is a transition between these limiting characteristics for the region $0.2r_p \le m_h \le 0.5r_p$.

Figure 4 (d) shows full voltammograms for different concentrations of supporting electrolyte concentration. The limiting current decreases as the supporting electrolyte concentration increases for the simulated case of $FcTMA^+$ being oxidized to $FcTMA^{2+}$, because the product with z = 2+, generated at the working electrode, has an increasingly negligible influence on the local electric field. It should be noted that the absolute effect of the supporting electrolyte concentration on the working electrode response is minimal.

For experimental measurements a probe of r_p = 0.6 μm and θ = 8.5° containing 2 mM $FcTMA^+$ and 50 mM KCl was employed. The tip−substrate separation was determined to be 0.15 μm from the direct and alternating current response (*vide supra*). The fraction of the applied experimental potential difference at faces A and B (in this case 0.44) was determined by matching the simulated barrel current, i_{ic}, to the experimental barrel current, i_b, for a potential difference of 0.2 V applied between the QRCEs. Figure 5 (a) and (b) shows that there is excellent agreement between the experimental (i_b) and FEM ion conductance current (i_{ic}) response over the applied bias range of 0.1−0.5 V. A linear (ohmic) response of the migration current to bias potential (E_b) was observed.

Figure 5 (c) and (d) shows experimental cyclic voltammetry and steady-state currents for E_b in the range 0 to 0.5 V with the corresponding FEM modeling data, measured simultaneously with the ion conductance responses. It can be seen that the working electrode current increases with increasing pipet bias potential and that there is less hysteresis between the forward and reverse voltammetry responses as E_b increases. This is because increasing E_b serves to increase the migration of $FcTMA^+$ toward the working electrode surface as a consequence of the larger potential gradient experienced by the charged species, thereby enhancing mass transport. When no bias is applied between the QRCEs, E_b = 0 V, mass transport to the working electrode is purely by diffusion, and one sees a clear hysteresis between the forward and reverse scan, which is evidently characterized by nonsteady-state diffusion for most of the voltammogram. Here, an experimental potential difference of 0.5 V between the QRCEs provides a 3-fold enhancement of the mass transport-limited current, highlighting that both migration and diffusion within the pipet contribute significantly to the working electrode response. Thus, one can change the potential between the two QRCEs to vary and control mass transport of charged species, and so investigating the importance of mass transport in an electrochemical process with one pipet. A further interesting consequence of the theta pipet geometry is that mass transport can be directional and asymmetric with respect to the 2 barrels as outlined in detail in the Supporting Information S3. Figure 5 (c) and (d) indicates good agreement between the experimental and simulated data

dx.doi.org/10.1021/ac203195h | *Anal. Chem.* XXXX, XXX, XXX−XXX

for the working electrode limiting currents over the entire range of bias potentials.

Figure 5 (e) shows that there is a subtle change in i_b for the experimental data during a CV measurement. Note that the raw data, as presented in (e), is overwhelmingly due to ion conductance but also has a very minor contribution from the counter electrode reaction (at the most driving QRCE) to the working electrode process, which can reliably be accounted for. Thus, the change in the ion-conductance current during a CV can be derived from the experimental i_b and i_{WE} responses and compared to the simulated change in i_{ic} as in Figure 5 (f), which shows that the trend in the simulated data and experimental data are in good agreement.

The process considered here was found to be reversible, consistent with experiments[28] and simulations presented in the Supporting Information. The range of kinetics that can be reached with a singly charged species and micrometer scale pipet tip is estimated to be *ca.* 0.1−1 cm s^{-1}, as shown in section S3 of the Supporting Information.

CONCLUSIONS

In this paper we have shown that mass transport and surface kinetics in SECCM can be described quantitatively by FEM modeling. This treatment provides a foundation for the future use of this technique for kinetic measurements at a range of interfaces and in high resolution voltammetric imaging. Notably, the simulations have provided insights into the relative contribution of diffusion and migration in the SECCM configuration. The simulations highlight the importance of knowing the pipet geometry (particularly tip radius and semiangle) with high precision for the quantitative analysis of data. These dimensions can be readily obtained by FE-SEM measurements. The geometry of solution between the tip and the surface has relatively little influence on both the migration current and mass transport to the substrate, but the influence of this region increases with increasing pipet bias voltage for the working electrode response for a charged redox-active molecule. We have shown how the meniscus dimensions, particularly the height, can be determined by tip approach measurements coupled with FEM, providing a means of accurately characterizing SECCM systems. The meniscus radius has less influence on the SECCM response unless the wetting of the substrate is very poor. We have shown through imaging experiments (see Supporting Information Figure S1) that a good rule of thumb is that the meniscus wets surfaces encountered hitherto with a dimension similar to the pipet. In the future, techniques such as surface capacitance might be useful for the elucidation of active surface areas, but as the capacitances will be very small, it may be challenging to avoid the influence of stray capacitance.

For pipets of the order of 1 μm diameter, as considered herein, SECCM has the capability to probe heterogeneous electron transfer processes with standard rate constants up to the range 0.1−1 cm s^{-1}. Further decreases in probe size and the use of high applied bias potentials will serve to increase this value. Work is in progress to implement much smaller probes.

The ability to measure both the working electrode and conductance currents simultaneously has been demonstrated, and we expect this could be very useful in the future in the study of the ingress and egress of ions in electrochemical processes, e.g. of polymer-modified (conducting, redox active) electrodes or of other solid-state electrode processes where coupled ion transfer is important. These properties, combined with the ability to accurately scan a surface and to locate the pipet precisely over an area of interest,[1,2] make SECCM a powerful new technique for surface and micro/nanoscale electrochemical investigations.

ASSOCIATED CONTENT

Supporting Information

Additional information is provided on pipet characterization, simulation details, and substrate electrode kinetics as referred to in the text. This material is available free of charge via the Internet at http://pubs.acs.org.

AUTHOR INFORMATION

Corresponding Author

*E-mail: p.r.unwin@warwick.ac.uk.

Notes

The authors declare no competing financial interest.

ACKNOWLEDGMENTS

M.E.S. and A.G.G. contributed equally to this work. The European Research Council has provided financial support under the European Community's (EC's) Seventh Framework Programme (FP7/2007-2013)/ERC-2009-AdG2471143-QUANTIF. A.G.G. and S.C.S.L. were further supported by EC (FP7/2007-2013) Marie Curie Intra-European Fellowships (projects: 236885 "FUNSENS"; and 275450 "VISELCAT"). Further support from EPSRC for studentships to K.M. (MOAC Doctoral Training Centre), N.E. (CTA scheme with the National Physical Laboratory, UK), and M.A.O.'C. (CTA scheme with Syngenta) is acknowledged. Some of the equipment used in this work was obtained through the Science City Advanced Materials project with support from Advantage West Midlands and the European Regional Development Fund.

REFERENCES

(1) Ebejer, N.; Schnippering, M.; Colburn, A. W.; Edwards, M. A.; Unwin, P. R. *Anal. Chem.* **2010**, *82*, 9141.

(2) Lai, S. C. S.; Dudin, P. V.; Macpherson, J. V.; Unwin, P. R. *J. Am. Chem. Soc.* **2011**, *133*, 10744.

(3) Bard, A. J.; Mirkin, M. V. *Scanning Electrochemical Microscopy*; Marcel Dekker: New York, 2001.

(4) Amemiya, S.; Bard, A. J.; Fan, F.-R. F.; Mirkin, M. V.; Unwin, P. R. *Annu. Rev. Anal. Chem.* **2008**, *1*, 95.

(5) (a) Bard, A. J.; Fan, F. R. F.; Kwak, J.; Lev, O. *Anal. Chem.* **1989**, *61*, 132. (b) Kwak, J.; Bard, A. J. *Anal. Chem.* **1989**, *61*, 1221. (c) Bard, A. J.; Fan, F.-R. F.; Pierce, D. T.; Unwin, P. R.; Wipf, D. O.; Zhou, F. *Science* **1991**, *254*, 68.

(6) (a) Macpherson, J. V.; Unwin, P. R. *Anal. Chem.* **2000**, *72*, 276. (b) Kranz, C.; Friedbacher, G.; Mizaikoff, B. *Anal. Chem.* **2001**, *73*, 2491. (c) Macpherson, J. V.; Unwin, P. R. *Anal. Chem.* **2001**, *73*, 550. (d) Macpherson, J. V.; Unwin, P. R.; Hillier, A. C.; Bard, A. J. *J. Am. Chem. Soc.* **1996**, *118*, 6445. (e) Dobson, P. S.; Weaver, J. M. R.; Burt, D. P.; Holder, M. N.; Wilson, N. R.; Unwin, P. R.; Macpherson, J. V. *Phys. Chem. Chem. Phys.* **2006**, *8*, 3909. (f) Kueng, A.; Kranz, C.; Lugstein, A.; Bertagnolli, E.; Mizaikoff, B. *Angew. Chem., Int. Ed.* **2003**, *42*, 3238. (g) Kueng, A.; Kranz, C.; Lugstein, A.; Bertagnolli, E.; Mizaikoff, B. *Angew. Chem., Int. Ed.* **2005**, *44*, 3419.

(7) (a) Hengstenberg, A.; Kranz, C.; Schuhmann, W. *Chem.—Eur. J.* **2000**, *6*, 1547. (b) Lee, Y.; Ding, Z. F.; Bard, A. J. *Anal. Chem.* **2002**, *74*, 3634. (c) Buchler, M.; Kelley, S. C.; Smyrl, W. H. *Electrochem. Solid St.* **2000**, *3*, 35. (d) Takahashi, Y.; Shiku, H.; Murata, T.; Yasukawa, T.; Matsue, T. *Anal. Chem.* **2009**, *81*, 9674.

(8) (a) Katemann, B. B.; Schulte, A.; Calvo, E. J.; Koudelka-Hep, M.; Schuhmann, W. *Electrochem. Commun.* **2002**, *4*, 134. (b) Katemann, B. B.; Inchauspe, C. G.; Castro, P. A.; Schulte, A.; Calvo, E. J.;

Schuhmann, W. *Electrochim. Acta* **2003**, *48*, 1115. (c) Horrocks, B. R.; Schmidtke, D.; Heller, A.; Bard, A. J. *Anal. Chem.* **1993**, *65*, 3605. (d) Alpuche-Aviles, M. A.; Wipf, D. O. *Anal. Chem.* **2001**, *73*, 4873. (e) Baranski, A. S.; Diakowski, P. M. *J. Solid State Electrochem.* **2004**, *8*, 683. (f) Ervin, E. N.; White, H. S.; Baker, L. A. *Anal. Chem.* **2005**, *77*, 5564. (g) Ervin, E. N.; White, H. S.; Baker, L. A.; Martin, C. R. *Anal. Chem.* **2006**, *78*, 6535. (h) Kurulugama, R. T.; Wipf, D. O.; Takacs, S. A.; Pongmayteegul, S.; Garris, P. A.; Baur, J. E. *Anal. Chem.* **2005**, *77*, 1111. (i) Diakowski, P. M.; Ding, Z. *Phys. Chem. Chem. Phys.* **2007**, *9*, 5966.

(9) (a) McKelvey, K.; Edwards, M. A.; Unwin, P. R. *Anal. Chem.* **2010**, *82* (15), 6334. (b) McKelvey, K.; Snowden, M. E.; Peruffo, M.; Unwin, P. R. *Anal. Chem.* **2011**, *83*, 6447.

(10) (a) Takahashi, Y.; Shevchuk, A. I.; Novak, P.; Murakami, Y.; Shiku, H.; Korchev, Y. E.; Matsue, T. *J. Am. Chem. Soc.* **2010**, *132*, 10118. (b) Comstock, D. J.; Elam, J. W.; Pellin, M. J.; Hersam, M. C. *Anal. Chem.* **2010**, *82*, 1270. (c) Takahashi, Y.; Shevchuk, A. I.; Novak, P.; Zhang, Y.; Ebejer, N.; Macpherson, J. V.; Unwin, P. R.; Pollard, A. J.; Roy, D.; Clifford, C. A.; Shiku, H.; Matsue, T.; Klenerman, D.; Korchev, Y. E. *Angew. Chem., Int. Ed.* **2011**, *50*, 9638.

(11) (a) Momotenko, D.; Cortes-Salazar, F.; Lesch, A.; Wittstock, G.; Girault, H. H. *Anal. Chem.* **2011**, *83*, 5275. (b) Lohrengel, M. M.; Moehring, A.; Pilaski, M. *Electrochim. Acta* **2001**, *47*, 137. (c) Hassel, A. W.; Lohrengel, M. M. *Electrochim. Acta* **1997**, *42*, 3327. (d) Spaine, T. W.; Baur, J. E. *Anal. Chem.* **2001**, *73*, 930.

(12) (a) Williams, C. G.; Edwards, M. A.; Colley, A. L.; Macpherson, J. V.; Unwin, P. R. *Anal. Chem.* **2009**, *81*, 2486. (b) Yang, D.; Han, L.; Yang, Y.; Zhao, L.-B.; Zong, C.; Huang, Y.-F.; Zhan, D.; Tian, Z.-Q. *Angew. Chem., Int. Ed.* **2011**, *50*, 8679.

(13) (a) Suter, T.; Bohni, H. *Electrochim. Acta* **1997**, *42*, 3275. (b) Suter, T.; Bohni, H. *Electrochim. Acta* **1998**, *43*, 2843.

(14) (a) Rodolfa, K. T.; Bruckbauer, A.; Zhou, D. J.; Korchev, Y. E.; Klenerman, D. *Angew. Chem., Int. Ed.* **2005**, *44*, 6854. (b) Shevchuk, A. I.; Gorelik, J.; Harding, S. E.; Lab, M. J.; Klenerman, D.; Korchev, Y. E. *Biophys. J.* **2001**, *81*, 1759. (c) Shevchuik, A. I.; Frolenkov, G. I.; Sanchez, D.; James, P. S.; Freedman, N.; Lab, M. J.; Jones, R.; Klenerman, D.; Korchev, Y. E. *Angew. Chem., Int. Ed.* **2006**, *45*, 2212.

(15) (a) Laslau, C.; Williams, D. E.; Wright, B. E.; Travas-Sejdic, J. *J. Am. Chem. Soc.* **2011**, *133*, 5748. (b) Chen, C.-C.; Zhou, Y.; Baker, L. A. *ACS Nano* **2011**, *5*, 8404. (c) Chen, C.-C.; Derylo, M. A.; Baker, L. A. *Anal. Chem.* **2009**, *81*, 4742.

(16) Wei, C.; Bard, A. J.; Nagy, G.; Toth, K. *Anal. Chem.* **1995**, *67*, 1346.

(17) Shao, Y.; Mirkin, M. V. *Anal. Chem.* **1998**, *70*, 3155.

(18) Szentirmay, M. N.; Martin, C. R. *Anal. Chem.* **1984**, *56*, 1898.

(19) Bartle, K. D.; Myers, P. *J. Chromatogr., A* **2001**, *916*, 3.

(20) (a) White, H. S.; Bund, A. *Langmuir* **2008**, *24*, 12062. (b) Wang, G. L.; Zhang, B.; Wayment, J. R.; Harris, J. M.; White, H. S. *J. Am. Chem. Soc.* **2006**, *128*, 7679.

(21) Lide, R. *CRC Handbook of Chemistry and Physics*; CRC Press: USA, 2001.

(22) Bertoncello, P.; Ciani, I.; Li, F.; Unwin, P. R. *Langmuir* **2006**, *22*, 10380.

(23) Newman, J. S.; Thomas-Alyea, K. E. *Electrochemical Systems*; Wiley-Interscience: 2004; pp 271−295.

(24) Bard, A. J.; Faulkner, L. R. *Electrochemical Methods*, 2nd ed.; John Wiley and Sons: New York, 2001.

(25) Rodolfa, K. T.; Bruckbauer, A.; Zhou, D. J.; Schevchuk, A. I.; Korchev, Y. E.; Klenerman, D. *Nano Lett.* **2006**, *6*, 252.

(26) Heinze, J. *J. Electroanal. Chem.* **1981**, *124*, 73.

(27) Edwards, M. A.; Williams, C. G.; Whitworth, A. L.; Unwin, P. R. *Anal. Chem.* **2009**, *81*, 4482.

(28) (a) Dumitrescu, I.; Dudin, P. V.; Edgeworth, J. P.; Macpherson, J. V.; Unwin, P. R. *J. Phys. Chem. C* **2010**, *114*, 2633. (b) Dumitrescu, I.; Unwin, P. R.; Wilson, N. R.; Macpherson, J. V. *Anal. Chem.* **2008**, *80*, 3598.